Chaos, Complexity and Transport

Marseille, France 23 – 27 May 2011

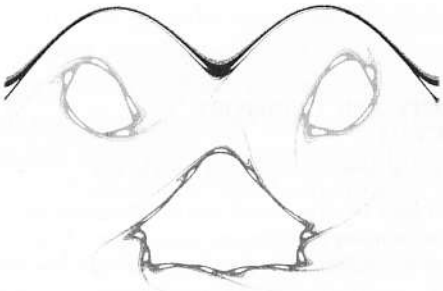

edited by

Xavier Leoncini
Aix-Marseille Université, France

Marc Leonetti
CNRS, France

World Scientific

NEW JERSEY · LONDON · SINGAPORE · BEIJING · SHANGHAI · HONG KONG · TAIPEI · CHENNAI

Published by

World Scientific Publishing Co. Pte. Ltd.

5 Toh Tuck Link, Singapore 596224

USA office: 27 Warren Street, Suite 401-402, Hackensack, NJ 07601

UK office: 57 Shelton Street, Covent Garden, London WC2H 9HE

British Library Cataloguing-in-Publication Data

A catalogue record for this book is available from the British Library.

CHAOS, COMPLEXITY AND TRANSPORT

Proceedings of the CCT '11

ISBN 978-981-4405-63-8

Printed in Singapore by B & Jo Enterprise Pte Ltd

SPIRAL PATTERN FORMATION IN A SIMPLE TWO-PHASE FLOW SYSTEM

H. N. YOSHIKAWA*, C. MATHIS, P. MAÏSSA and G. ROUSSEAUX

Laboratoire J.-A. Dieudonné, UFR 6621 CNRS,
Université de Nice Sophia-Antipolis,
Parc Valrose – 06108 Nice Cedex 2, France, European Union
**E-mail: Harunori.Yoshikawa@gmail.com*

A spiral pattern formation in a gas–liquid two phase flow is investigated experimentally. Bubbles are injected periodically into a liquid layer with a free surface and emerge one by one from the surface to exhibit regular arrangements. These arrangements are characterized by a constant angular shift in the direction of bubble radial motion after the emergence. A transition from the regime with a shift of 180 degrees to the regime of smaller angles is found. Observation of bubble behavior shows that the compaction among emerging elements (bubbles) plays an important role in the pattern formation, as in the development of regular leaf arrangement around a plant stem, the phyllotaxis. A theoretical model including the flow advection and the bubble–bubble interaction is developed to get deeper insights into the pattern generation. It is found the model reproduces different patterns and the transition between the two regimes.

Keywords: Pattern formation, Phyllotaxis, Two-phase flow.

1. Introduction

A simple two-phase flow system in which bubbles are formed by continuous gas supply through a tube or an orifice is known to be rich in bubble dynamical behavior.[1,2] In the present paper, we report an experimental and theoretical work on a pattern formation in this two-phase flow system with a free surface (Fig. 1.1a). Nitrogen gas is injected into a viscous liquid through an orifice of typically 0.8 mm at the center of the bottom of a vertical cylindrical tank to form bubbles periodically. The liquid is a silicone oil and the bubbles have typically a volume-equivalent diameter $D_e \approx 6$ mm. After their release at the orifice, bubbles rise due to the buoyancy in a regular chain. This bubble motion induces a jet along the bubble rising path, which impinges the free surface to make a bump (apex) and is converted into a

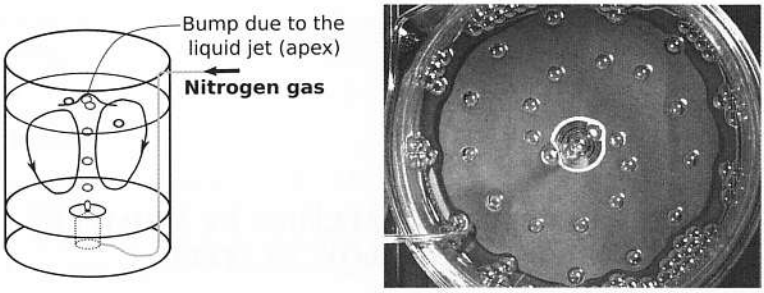

(a) (b)

Fig. 1.1. Illustration of the experimental setup (a) and a typical pattern formed by bubbles on the free surface (b). The liquid is a silicone oil of 3.5×10^{-5} m^2/s in (b).

diverging surface flow. Bubbles emerge from the apex and are advected radially by the surface flow.

At small gas flow rate Q, emerged bubbles are clustered at the surface central zone due to the capillary force between bubbles. With increasing Q, the advection by the surface flow and the frequency of bubble injection, $1/T$, become important, where T is the period of bubble formation. Each emerged bubble then moves individually in a radial direction at the surface. The angle of divergence, ψ, *i.e.*, the angular shift between the radial directions of consecutive bubbles, is constant and equal to 180 degrees. In this *distichous regime*, a straight arrangement of bubbles is observed on the surface. Further increase of Q leads to another regime, *spiral regime*, where ψ is a constant smaller than 180 degrees: a spiral arrangement is formed at the surface, as seen in Fig. 1.1b. The transition between these two regimes occurs through a supercritical bifurcation (Fig. 1.2a). For a variety of formed spirals and more complete description of the experimental setup, see Yoshikawa *et al.*[3]

Spirals that result from a constant angular shift between consecutive elements are also found in the arrangement of leaves around a plant stem. This arrangement, called *phyllotaxis*, is known by its mathematical richness and has attracted scholars by its relation with the golden mean $\tau = \left(\sqrt{5}+1\right)/2$ and the Fibonacci series. Microscopic observation and surgical experiments to shoot apexes where leaf primordia are born suggest that the compaction of the primordia during the meristematic development plays a main role in the phyllotaxis.[4] Recent works done in the context of non-linear physics show that repulsing elements subjected to a geometrical constraint can ex-

hibit patterns characterized by a constant angular shift between consecutive elements.[5–7] Transition from the distichous to spiral arrangements is found when increasing the compaction. Further increase of the compaction leads to successive quasi-bifurcations. In these quasi-bifurcations, there is only one route that can be followed continuously from the distichous regime. It converges to the Fibonacci angle $\psi_F = 360°/\tau^2 = 137.5°$, which is regarded as the most frequently observed angle in natural plants. These results indicate that the phyllotactic pattern formation constitutes a wide class of pattern formation in different physical and biological systems.

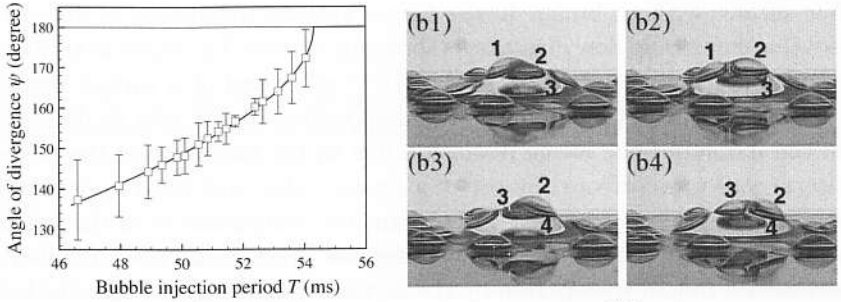

Fig. 1.2. Behavior of the angle of divergence ψ (a) and successive images showing bubble behavior at their emergence from the free surface in the spiral regime (b). In (b), the bubbles are numbered chronologically. The liquid is a silicone oil of 3.5×10^{-5} m^2/s.

In our two-phase flow system, close approach of bubbles occurs in the apex. Two bubbles are close together at their emergence in the distichous regime. In contrast, three bubbles are seen together in the spiral regime, *e.g.*, (b2) and (b4) in Fig. 1.2. This observation suggests that a formed pattern is a result of packing of the elements that are subjected to a geometrical constraint due to the flow stagnation. The behavior of ψ and the latter observation suggest that the pattern formation mechanism is similar to phyllotaxis.

In the next section, we characterize the flow induced by the bubble ascending motion. Results of velocity field measurements by the Particle Image Velocimetry (PIV) technique are used to obtain a simple analytical expression of the flow in the apex and estimate related parameters. We then develop a theoretical model in Sec. 3. Forces that represent different contributions in the pattern formation are balanced in order to construct the model phenomenologically. Numerical simulations of the model

are presented in Sec. 4. We will see that the model reproduce properly our experimental observations.

2. Flow and bubble motion

Global flow is induced in the tank by the bubble ascending motion. It consists of a jet along the center axis, a surface flow and a recirculation. The jet impinges the free surface and deforms it to yield an apex, as seen in pictures in Fig. 1.2b. The jet is then converted into the surface flow diverging from the center. Figure 2.1a shows a velocity field determined by the PIV technique. The horizontal plane $z = 0$ is coincident with the free surface without bump. In the figure, velocity magnitude is shown by isovalue curves and flow direction is shown by arrows. The liquid is a silicone oil of a kinematic viscosity $\nu = 3.5{\times}10^{-5}$ m^2/s and of a surface tension $\gamma = 0.02$ N/m. It is contained in a glass beaker of 130 mm in diameter. In the measurement, image distortion due to the curvature of the beaker lateral wall was corrected by use of a square outer tank filled by water. In the figure, it is seen that a jet of a diameter comparable with the bubble size is converted into a surface diverging flow. The jet Reynolds number is around 40. Liquid transported by the surface flow is returned into the bulk by a recirculation, as illustrated in Fig. 1.1a. The latter is much weaker than the jet and the surface flow: typically, the velocities of the jet, the surface flow and the recirculation are of the order of 0.2 m/s, 0.2 m/s and 0.01 m/s, respectively.

Bubbles released at the bottom orifice move in this global flow. They ascend in a regular chain inside the jet with a constant velocity until the emergence from the free surface. Relative velocity ΔU of rising bubbles to the jet is typically 0.1 m/s, giving the bubble Reynolds number $Re_b = \Delta U D_e/\nu$ of the order of 20. Near the surface, rising bubbles are decelerated and caught up by followers due to the stagnation of the flow. Close approach of bubbles then occurs. The number of bubbles in this approaching event seems to play an important role in the pattern generation mechanism, as mentioned to in Sec. 1. It is therefore essential to characterize the flow near the stagnation point, *i.e.*, $r = 0$ on the free surface.

Near the surface, *i.e.* $z \approx 0$, the jet profile is affected by the boundary condition at the free surface and by the presence of the apex. In Fig. 2.1b, the profile of the jet vertical velocity field U_z is shown for different vertical positions. The measurement was done after flow perturbation by a bubble passage was relaxed. The next rising bubble was far below to influence the measured flow (its upper surface is at $z = -5.4$ mm). It is seen in

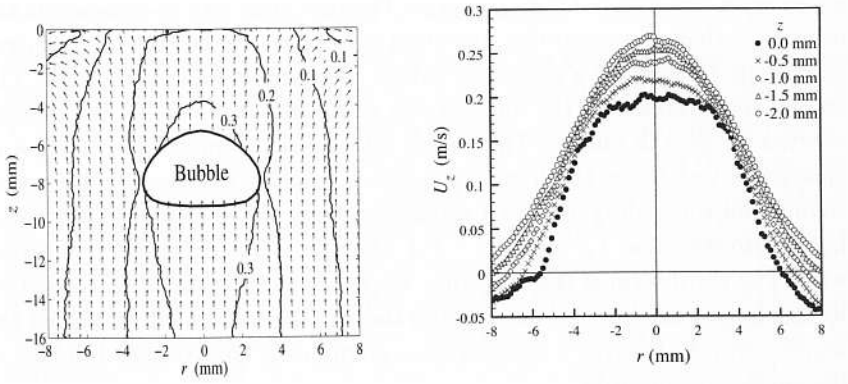

(a) (b)

Fig. 2.1. Velocity field below the free surface (a) and profiles of vertical velocity at different vertical positions (b). The liquid is a silicone oil of 3.5×10^{-5} m^2/s. The flow rate of gas injection is 2070 mm^3/s.

the figure that the nose of the jet becomes flattened when approaching to the surface. In the proximity of the center axis, we can develop the vertical velocity field U_z into a power series of r^2 due to the symmetry: $U_z = V_0 + V_2 r^2 + \cdots$. The coefficients $V_0, V_1, \ldots$ are functions of z. As seen in Fig. 2.1b, the velocity at the jet nose V_0 decreases linearly with the vertical position: $V_0 = -2az + b$. The constant a is the radial gradient of the radial velocity U_r at the center. Indeed, use of the continuity equation gives $U_r = -r^{-1} \int r U_z dr = ar + O(r^3)$. The constant b is associated with the presence of the apex. For the flow in Fig. 2.1b, $a = 20$ s^{-1} and $b = 0.19$ m/s. This approximative velocity field will be used to model the bubble behavior in the apex in the next section.

3. Theoretical model

As discussed earlier, interaction between bubbles moving in the stagnation flow in the apex seems to be responsible for the observed regular bubble arrangement on the surface. Taking essential aspects into account, we developed a theoretical model consisting of the following set of equations of motion:

$$0 = 2\pi\rho\nu D_e \left(\boldsymbol{U} - \frac{d\boldsymbol{r}_j}{dt} \right) + \sum_i \mathbf{f}_{ji} + \rho \frac{\pi}{6} D_e^3 g \boldsymbol{e}_z + \boldsymbol{S} \quad (j = 1, 2, \ldots), \quad (1)$$

where $\boldsymbol{r}_j$ is the j'th bubble's position. The first term in the equation is the drag force that represents the advection of bubbles by the flow $\boldsymbol{U}$. The drag coefficient $16/Re_b$ for a spherical bubble in creeping flow is adopted. The second term represents the interactions with other bubbles: $\mathbf{f}_{ji}$ is the force exerted by the i'th bubble. The bubble interaction occurs at the moment of emergence just below the free surface where bubbles approach to their preceding and succeeding ones in a stagnation flow. We model this interaction by the Hooke's law: $\mathbf{f}_{ji} = K(\boldsymbol{r}_j - \boldsymbol{r}_i)$ when $|\boldsymbol{r}_j - \boldsymbol{r}_i| < D_e$; $\mathbf{f}_{ji} = 0$ otherwise. The third term is the buoyancy force due to the gravity. A correction to this force after bubbles emerge and the surface tension effect consist the fourth term $\boldsymbol{S}$. It gives a vertical force component that pushes bubbles at the surface downwards.

In the experiment, the angle of divergence ψ is decided at the emergence of bubbles. Considering the bubble motion only within the apex, *i.e.*, $r \approx 0$ and $z \approx 0$, we suppose the flow velocity field is given by $U_r = ar$ and $U_z = -2az + b$, as discussed in the preceding section. For simplicity, we will neglect the influence of the apex height and set $b = 0$ in the model throughout the present paper.

Nondimensionalizing Eq. (1) with a time scale T and a length scale D_e, we get the following coupled ordinary equation set:

$$\frac{d\boldsymbol{r}_j}{dt} = A\boldsymbol{U} + F\sum_{j\neq i}(\boldsymbol{r}_j - \boldsymbol{r}_i)\,H\left(1 - |\boldsymbol{r}_j - \boldsymbol{r}_i|\right) + S\left(Bo, G\right)\boldsymbol{e}_z \qquad (2)$$

where H stands for the Heaviside step function. The dimensionless parameters A and F represent the advection by the flow and the bubble–bubble interaction, respectively: $A = aT$ and $F = KT/2\pi\rho\nu D_e$. For the silicone oil of 3.5×10^{-5} m^2/s, the transition from the distichous to spiral regimes occurs at around $T = 54$ ms (see Fig. 1.2a). The parameter a is of the order of 20 s^{-1}, as shown in Sec. 2. The advection parameter A is hence of the order of 1 at the transition. In the definition of F, we do not know the exact nature of the stiffness K. Assuming the repulsive interaction is associated with the restoration of deformed bubbles due to the capillary pressure, we could estimate the stiffness by $K \sim \gamma$. It gives a value of the order of unity to F: we will set F at 0.3 in the present paper. The term S includes the Bond number $Bo = \rho D_e^2 g/\gamma$ and a dimensionless gravity $G = gD_eT/12\nu$. We will fix these parameters at their typical experimental values $Bo = 17$ and $G = 7.6$.

4. Results of the simulation of the model

Numerical simulation of the model is carried out by integrating the ordinary differential equation set (2) with the initial condition that j'th bubble ($j = 1, 2, \ldots$) is injected at $z = z_0$ with a velocity v_0: $\boldsymbol{r}_j = z_0 \boldsymbol{e}_z$ and $d\boldsymbol{r}_j/dt = v_0$ at $t = j - 1$. The typical values of z_0 and v_0 are -3 and 0, respectively. The fourth-order Runge–Kutta method with a step $\Delta t = 0.05$ was adopted for the integration. The simulation shows that bubbles can be in contact and interact with others only when they are emerging from the surface at a small central zone ($r \lesssim 1$). After going out from this zone, bubbles move in radial directions with no more interaction with others. We can then determine the radial direction of each bubble's motion. Figure 4.1a shows a typical behavior of the divergence θ_j between j'th and $(j+1)$'th bubbles ($j = 1, 2, \ldots, 100$) for $A = 0.6$. It is seen that the divergence converges to a constant value after an initial transient phase over around 50 bubbles. The final value of the divergence, ψ, is 160 degrees: a spiral arrangement will be formed on the free surface. In the figure, the number N_j of the bubbles with which the bubble j interacts is also plotted. This number can be counted by following the positions of all bubbles during the simulation, without ambiguity because of our hypothesis of a Hooke-type law for the interaction. While N_j takes odd values (3 and then 5) at the beginning, it converges to the final even value $N = 4$ after thirty bubbles. Note that $N = 4$ means each bubble interacts with two preceding and two succeeding bubbles. Close approach of three bubbles will be observed in the apex. This corresponds well to our experimental observation in the spiral regime.

The final value of the divergence, ψ, depends on the advection parameter A and the interaction parameter F. Varying these values, indeed, we can find that the model can also reproduce the bifurcation from the distichous to spiral regimes observed in the experiment. Figure 4.1b shows the behavior of ψ when the advection parameter A is varied. The interaction parameter F is fixed as $F = 0.3$. For large A, the divergence ψ is equal to 180 degrees and the system is in the distichous regime. Below a critical value $A_{cr} = 0.66$, ψ decreases with decreasing A. This behavior is similar to that observed in the experiment (see Fig. 1.2a), where ψ decreases with decreasing the bubble injection period T. Furthermore, $A_{cr} = 0.66$ is the same order of magnitude of the experimentally estimated A (~ 1, see Sec. 2). Further decrease of A leads to another transition at $A = 0.34$, where ψ starts to increase. This transition seems similar to the first quasi-bifurcation from the branch (1, 2) to the branch (2, 3), found in the theoretical studies on phyllotactic pattern formation,[5,6] where (n, m) means the parastichy number often used

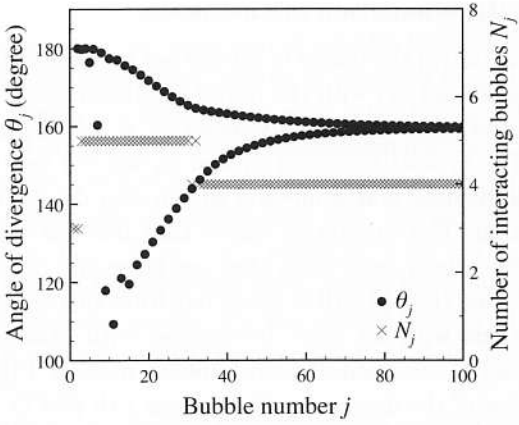

(a)

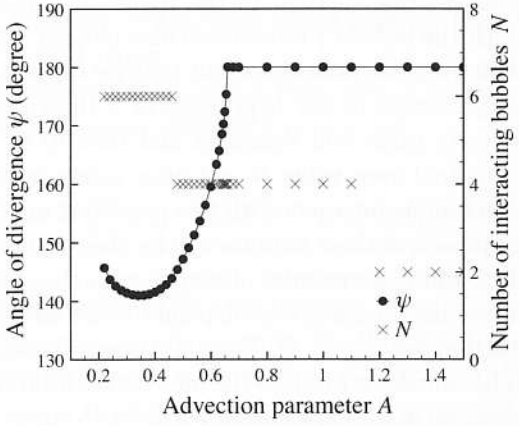

(b)

Fig. 4.1. Behavior of the angle of divergence θ_j (a) and its final constant values ψ for different advection parameter A (b). The bubble interaction number N_j and its final value N are also shown in these graphs. The interaction parameter F is fixed at $F = 0.3$.

in the phyllotaxis analysis. In Fig. 4.1b, the interacting bubble number N is also plotted. For large A, N is equal to 2: each emerging bubble interacts with its preceding one as well as its succeeding one. This means that, in the apex, only two bubbles are close together in each interaction. With decreasing A, the number N jumps to 4: the bubble j interacts with the

bubbles $j-2$, $j-1$, $j+1$ and $j+2$. However, the interactions with the bubbles $j \pm 2$ are not strong enough to modify the pattern: it stays in the distichous mode. The transition to the spiral mode takes place later at a smaller $A(=A_{cr})$, when these interactions become effective. This agrees with the experimental observation that three bubbles are close together in the apex in the spiral regime. Further decrease of A gives another jump of N to 6. This precedes the transition from the $(1,2)$ to $(2,3)$ branches: the latter occurs at $A=0.34$ when the interactions of the bubble j with the bubbles $j \pm 3$ become effective. In the experiment, the branch $(2,3)$ was not observed: instability of ascending bubble chain[8] occurs below a certain value of $T=T_1$ before close approach of four bubbles is observed in the apex ($T_1 \approx 46$ ms in the case of Fig. 1.2a). No regular spiral pattern is then seen on the surface. As these observations show, the simple model (2) reproduces essential features of our experiment.

5. Conclusion

We investigated a spiral pattern formation by periodically emerging bubbles from a liquid free surface. Experimental observation of bubble behavior showed that the bubble–bubble interaction in a bump of the surface (apex) plays an essential role in the formation of pattern. This indicates the analogy with the meristematic development in a shoot apex of plants resulting in a regular leaf arrangement. A simple phenomenological model was developed for our experimental system by taking into account the advection by the liquid flow and the bubble–bubble interaction, both of which affect the compaction of bubbles in the apex. Velocity field measurements by the PIV technique were used to model the flow and estimate the magnitude of an advection parameter A. Numerical simulation of the model showed that it reproduced two important observations in the experiment, *i.e.*, the behavior of the angle of divergence ψ and the increase of interacting bubbles in the apex. The critical value of A agrees favorably with the experimental estimation.

We are carrying out a further exploration of the model. The parameter dependence of the system behavior is being investigated over a wide range of A and F and different types of interaction force is being examined. Comparisons of the model with the experiment are also being tried, including experimental estimations of the critical A for different liquids with different viscosities.

Acknowledgments

The financial supports from Région PACA, Conseil Général 06 and Fédération Wolfgang Doeblin are acknowledged with appreciation. H.N.Y. thanks Université de Nice Sophia-Antipolis for his post-doctoral grant.

References

1. E. Colli, V. S. M. Piassi, A. Tufaile and J. C. Sartorelli, *Phys. Rev. E* **70**, 066215 (2004).
2. V. S. M. Piassi, A. Tufaile and J. C. Sartorelli, *Chaos* **14**, 477 (2004).
3. H. N. Yoshikawa, C. Mathis, P. Maïssa, G. Rousseaux and S. Douady, *Eur. Phys. J. E* **33**, 11 (2010).
4. T. Sachs, *Pattern formation in plant tissues* (Cambridge University Press, 1991). Chap. 11.
5. L. S. Levitov, *Phys. Rev. Lett.* **66**, 224 (1991).
6. S. Douady and Y. Couder, *Phys. Rev. Lett.* **68**, 2098 (1992).
7. S. Douady and Y. Couder, *J. Theor. Biol.* **178**, 255 (1996).
8. M. C. Ruzicka, *Int. J. Multiphase Flow* **31**, 1063 (2005).